Pro-atherogenic diet accelerates tumor growth in mice through IL-1β and myeloid cell-derived VEGF-A

Thi Tran
INSERM U970/Université Paris Descartes
Bruno Esposito
Inserm U970
Melanie Montabord
Inserm U970
Jaouen Tran Rajau
Inserm U970
Nadege Gruel
Institute Curie
Olivia Lenoir
Paris Cardiovascular Centre, French Institute of Health and Medical Research https://orcid.org/0000-0001-8107-6987
Hafid Ait-Oufella
Inserm
Christian Stockmann
Institute of Anatomy, University of Zurich
Ziad Mallat
Division of Cardiovascular Medicine, University of Cambridge
Alain Tedgui
INSERM, Paris Cardiovascular Research Center
Eric Tartour
Inserm U970
Stephane Potteaux (stephane.potteaux@inserm.fr)
Inserm U976 https://orcid.org/0000-0003-3068-8769

Article

Keywords: Cardio-oncology, inflammation, monocytes, cancer, atherosclerosis, cytokines

Posted Date: October 20th, 2020

DOI: https://doi.org/10.21203/rs.3.rs-86825/v1

Abstract

Aims: Myeloid inflammatory cells are recruited to the tumor microenvironment and subsequently educated *in situ* to acquire a pro-invasive, pro-angiogenic and immunosuppressive phenotype. Components of the metabolic syndrome are known to aggravate tumorigenesis in part through myeloid cell activation. We hypothesized that consumption of a high fat/high cholesterol pro-atherogenic diet and its associated low-grade inflammation would accelerate the initiation of solid tumors.

Methods and results: Here, we show that two-week feeding of wildtype C57BL/6J mice with a pro-atherogenic diet increases the pool of circulating inflammatory Ly-6C^{hi} monocytes available for initial melanoma development and amplifies the accumulation of myeloid cells within the tumor microenvironment, in an IL-1β-dependent manner. Under pro-atherogenic diet feeding, myeloid cells display heightened pro-angiogenic, pro-inflammatory and immunosuppressive activities. Within the first days after tumor implantation, myeloid cells become the main producer of VEGF-A in the tumor. Depletion of Ly-6C^{hi} monocytes in mice fed with a pro-atherogenic diet limits immune cell infiltration in the tumor, and inhibits tumor growth. IL-1β deficiency or specific inhibition of VEGF-A in myeloid cells recapitulates the beneficial effect of Ly-6C^{hi} monocyte depletion, suggesting their complementary roles in tumorigenesis in the context of mild hyperlipidemia.

Conclusion: Our study shows that dyslipidemia provide high amounts of activated myeloid cells with pro-tumoral activity and shed light on cross-disease communication between cardiovascular pathologies and cancer.

Translational Perspective: In this study we demonstrate that dyslipidemia accelerates the development of solid tumors through the increased infiltration of Ly6C^{hi} monocytes that differentiate into pro-tumoral myeloid cells. These findings demonstrate that dyslipidemia can silently boost tumor development in normal-weight individuals through the action of IL-1β and VEGF-A. Our work sheds light on the potential benefit of targeting IL-1β and VEGF-A in cancer patients with moderate dyslipidemia.

Introduction

Metabolic syndrome (MS) is an established risk both for cancer and cardiovascular disease (CVD), the 2 leading causes of morbidity and mortality worldwide. Components of the MS include excess body fat, increased blood pressure, high blood sugar and dyslipidemia [1]. The metabolically unhealthy phenotype is defined by two or more of four of these components. In several types of cancers, dyslipidemia and obesity are associated with increased death rate [2,3]. This has also been functionally validated in experimental models of diet-induced obesity (DIO), which showed accelerated tumor growth [4,5]. Even though obesity is often associated with metabolic disorders, 24 to 30% of normal-weight adults are considered metabolically unhealthy, according to several worldwide meta-analyses [6,7]. These metabolically unhealthy normal weight individuals are commonly dyslipidemic. They present high circulating levels of cytokines and cardiometabolic risks comparable to those observed in metabolically

unhealthy obese individuals [8]. This highlights the need for a better understanding of the impact of MS and its individual components in tumorigenesis in normal-weight individuals. Dysfunctional fatty acid and cholesterol metabolism promotes tumor growth directly through activation of oncogenic signaling pathways and formation of lipid rafts [9,10], and indirectly through increased production and mobilization of monocytes [11,12].

Monocyte and monocyte-derived cells accumulate in many types of human and murine tumors and are thought to regulate several steps of tumor development, including antitumor T cell responses and angiogenic processes. Generally, high numbers/percentages of circulating monocytes indicate poor clinical prognosis in cancer [13], suggesting that the level of monocytes in blood may influence tumor development. In line with this hypothesis, it was recently shown that the peripheral count of monocytes was associated with the density of tumor-associated macrophages in colorectal cancer [14,15]. During inflammation, metabolic and epigenetic rewiring has been identified as important mechanisms of monocyte, and more generally myeloid cell, production and function [16]. Interleukin-1β (IL-1β), primarily generated by myeloid cells, functions as an upstream alarm capable of simultaneously regulating inflammation, mainly by inducing a local cytokine network and enhancing inflammatory cell infiltration to affected sites, and promoting angiogenesis, either directly or indirectly via induction of proangiogenic factors such as vascular endothelial growth factor A (VEGF-A) (reviewed in [17]). VEGF-A is produced by many cell types, including tumor cells and myeloid cells. As a major inducer of blood vessel growth, VEGF-A is involved in tissue remodeling in the context of cancer and cardiovascular diseases. In endothelial cells, VEGF-A and IL-1β share common signaling pathways and may synergistically regulate the expression of inflammatory genes and growth factors [18]. Anti-angiogenic agents and immunotherapies targeting VEGF-A are thought to create a transient window of vessel normalization, which might facilitate the diffusion of therapeutic agents [19,20]. Anti-IL-1β therapies, initially developed in the context of autoimmune diseases, have recently gained a great interest in the cardiovascular and oncology fields [21]. The major randomized trial on the role of IL-1β inhibition in atherosclerosis, named CANTOS, reported a reduction in the number of incident cases of lung cancer in patients treated with the anti-IL-1β antibody compared to placebo-treated patients [22]. This clinical study proposed that IL-1 antagonism could prevent both the recurrence of cardiovascular events and tumor development in patients with a persistent pro-inflammatory response.

Having reviewed the state of the art, we thought to evaluate the impact of mild-dyslipidemia-associated inflammation on solid tumor growth in mice. To address this question, we employed a high fat/high cholesterol atherogenic diet (HFHCD), known to increase lipid levels and induce systemic low-grade inflammation.

We found that 2-weeks feeding with HFHCD accelerated solid B16 melanoma development in C57BL/6J mice and induced an angiogenic and inflammatory signature in the tumor. Acceleration of tumor growth

was associated with increased Ly-6C^{hi} monocyte levels in blood and predominant accumulation of myeloid-derived cells in the growing tumor. Myeloid cells significantly contributed to the increase of VEGF-A in the tumor under HFHCD. IL-1β deficiency markedly reduced monocyte level in blood and subsequently stopped the expansion of tumors under HFHCD. Specific loss of myeloid-derived VEGF-A recapitulated the protective effect of systemic myeloid cell depletion in mice under HFHCD. This study shows that silent low-grade inflammation fuels early growing solid tumors with a pro-tumoral contingent of pre-educated myeloid cells via IL-1β production, and promote tumorigenesis through increased immunosuppression and VEGF-A synthesis.

Methods

Animals

All experiments were conducted according to European Community for experimental animal use guidelines (EC2010/63), and have been approved by the Ethical committee of University Paris Descartes (CEEA 34) and the French Ministry of Agriculture (agreement 17112). To investigate the effect of dyslipidemia on tumor development, we implanted the murine cancer lines in female C57BL/6J (River). OT-mice were also purchased from Charles River. IL-1β$^{-/-}$ mice were kindly given by Pr Yoichiro Iwakura (Tokyo University of Science, Japan). LysMCre$^{-/-}$VEGF^{f}/^{f} (WT) and LysMCre$^{+/-}$VEGF^{f}/^{f} (VEGF-A^{DLysM}) mice were provided by Dr Christian Stockmann. All mice were on C57BL/6J background.

Mouse breeding occurred in our animal facility in accordance with local recommendations. Control mice were matched with littermates of the appropriate, age, sex, and genetic background to account for any variation in data, when specified. Mice received a standard chow diet (Safe, A03) or pro-atherogenic high fat/high cholesterol diet (Ssniff, 15% cocoa butter and 1.25% cholesterol) and water ad libitum. Mouse euthanasia was performed by cervical dislocation after anesthesia with 4% isoflurane (IsoVet 100%; Centravet, France) in 100% oxygen in an anesthetic chamber which was not prefilled to prevent distress.

Total Cholesterol assay

Plasma cholesterol was measured using a commercial kit (DiaSys Cholesterol FS*, Germany).

Cell line and tumor challenge

The B16F10 and TC1 cells were purchased from ATCC (CRL6475, CRL2493). Cells were cultured in RPMI supplemented with 10% fetal bovine serum (FBS), 2 mM glutamine, 50 U/ml penicillin and 100µg/ml streptomycin (RPMI complete medium). Mice were subcutaneously (s.c) injected with $0.25x10^6$ B16-F10 or TC1 cells in 100µl of saline buffer in the shaved abdominal flank. Tumor growth was monitored every 2–3 days using a caliper until 15 days post-injection. Tumor size was calculated as: Width x Length in mm^2.

Cells isolation, staining and flow cytometry

Blood samples were collected by submandibular punction with 20-gauge needle under isofluorane anesthesia. Spleens were dissected and pressed through a 40-µM cell strainer, red blood cells were lysed with osmotic lysis buffer. Tumor were isolated from mice, minced and placed into GentleMACS C-tube with PBS-FCS 2%, dissociated mechanically with GentleMACS dissociator (Miltenyi) according to manufactor's standard protocol, then filtered on 70um strainer.

Single cell suspensions were first blocked with anti-CD16/32 antibody (93; eBioscience) and stained for surface molecules with the following antibodies in PBS-FCS 2%:

CD45 (30-F11 ; eBioscience), F4/80 (BM8;biolegend); CD11b (M1/70; eBioscience)

Ly6C (HK4.4; eBioscience), Ly6G (1A8, BD Biosciences), GR-1 (RB6-8C; Biolegend), CD8a (53-6.7; eBioscience), CD4 (GK1.5; eBioscience), CD3 (145-2C11; eBioscience), CD25 (PC61.5; eBioscience), NK1.1 (PK136; Biolegend). For intracellular staining of FoxP3, after surface staining, cells were permeabilized using the FoxP3/transcription Factor staining buffer set(eBioscience) according to manufactor's protocol, then stained with FoxP3 mAb (FJK-16S; eBioscience). Dead cells were excluded using live/dead fixable aqua dead cell kit (Invitrogen). Samples were acquired on Fortessa X20 and on a Fortessa Analyser (BD Biosciences) and analyzed with FlowJo software.

For Dimensionality reduction using t-SNE and automatic clustering : CD45 live cells were manually gated from multicolor flow cytometry and exported in a FCS file. t-Distributed Stochastic Neighbor Embedding (t-SNE) dimensionality reduction was performed using bh tsne, an implementation of t-SNE via Barnes-Hut approximations. 20 000 events were used for t-SNE dimensionality reduction.

Gene expression analysis

For the transcriptomic analysis, 4 tumors per group were harvested from mice fed with CD or HFHCD at Day 9 post injection of B16-F10 melanoma cells. Tumors were minced and lysed into RLT buffer

containing 1% β-mercaptoethanol. RNA was extracted using Qiagen RNeasy kit according to the manufacturer's instructions.

Analysis of gene was done by affymetrix microarrays at de GENOM'IC core facility (Cochin Institute)

In vivo cells labelling

A bead labeling technique was used to label monocytes in vivo, by retro-orbital i.v. injection of 1 µm fluorescent latex microbeads (YG, Polysciences) diluted ¼ in sterile PBS, on day 8 post tumor injection. Mice were sacrificed 24h later.

For intravital neutrophil and monocyte labeling, mice were retro-orbitally injected i.v with anti-Ly6G PE and anti-CD115 APC (5ug each) on day 8 post tumors injection. 6h later mice were sacrificed. Labeled cells were analyzed in blood and tumors by flow cytometry.

Culture in vitro

Bone marrow cells were collected from femurs and tibias by insertion of a needle into the bone and flushing with RPMI supplemented with 0.2% BSA and 1% FCS as previously described. Macrophages were differentiated after culture for 9 days with 20% L929 conditioned medium.

Splenocytes or BM-DM were cultured in RPMI 1640 supplemented with Glutamax, 10% FCS, 0.02 mmol/L β-mercaptoethanol and antibiotics Penicillin and Streptomycin. Cells were stimulated in RPMI complete medium with LPS (10µ g/ml, Sigma Aldrich)± mIFNg (100U/ml) then supernatent was harvested. IL-1b, IL-10, IL-12 or TNFa was measured by ELISA (R&D Systems).

For B16-F10 in vitro proliferation, 10 000 B16F10 cells were co-cultured with 2 500 CD45 cells isolated from tumors or with BM-DM, in RPMI complete medium. 24h later, B16F10 proliferation was measured by 3T-Thymidine incorporation or MTT assay (Sigma). For Thymidine incorporation one ìCi [^{3}H] thymidine was added to each well during the last 18 h. Thymidine incorporation was assessed using a TopCount NXT scintillation counter (Perkin Elmer).

Cytokines and chemokines assay, ELISA

Total protein from tumors was extracted using Bio-plex lysis buffer (Bio-Rad) according to manufactor's instructions, and concentration was determinated with BCA assay (Pierce).

CD45+ cells were isolated from fresh tumors by magnetic sort (Mojosort mouse CD45 nanobeads, Biolegend). Cells were cultured for 24h in RPMI complete medium then supernatent were harvested.

The bead-based multiplex immunoassay was used to measure the levels inflammatory and angiogenesis mediators from tumors protein lysates or from supernatant of CD45+ cells isolated from tumors. A 23-plex inflammatory immunoassay panel (IL-1α, IL-1β, IL-2, IL-3, IL-4, IL-5, IL-6, IL-9, IL-10, IL-12 (p40), IL-12 (p70), IL-13, IL-17A, Eotaxin, G-CSF, GM-CSF, IFN-γ, KC, MCP-1 (MCAF), MIP-1α, MIP-1β, RANTES, TNF-α) (Bio-Rad) and 5-plex angiogenesis immunoassay panel (PDFG-a, Endoglin, VEGFR2, Fas-L, ICAM-1)(R&D systems), were performed according to manufactor's protocol and analyzed on Bio-Plex 200 (Bio-rad). The analytes concentration was calculated using a standard curve (5 PL regression), with Bio-Plex manager software.

VEGF-a concentration was evaluated by ELISA (mouse VEGF DuoSet, R&D system) in tumors lysates and in plasma.

MDSC suppressive activity assay

MDSC ($CD11b^+$ $Ly6C^+$ $Ly6G^+$) enriched cells were obtained from spleen of tumor bearing mice by magnetic sort (Myeloid-Derived Suppressor Cell Isolation Kit, Miltenyi). CD8 T cells were isolated from spleen of OT-I mice by magnetic sort (CD8a+ T Cell Isolation Kit, Miltenyi), and labeled with 5uM CFSE (Vybrant™ CFDA SE Cell Tracer Kit, Invitrogen). OT-I CD8 T cells were incubated with $OVA_{257-264}$ (SIINFEKL) at 0.1ug/ml (Polypeptide) with various ratio of MDSC for 72h. On day 3, CFSE dilution was analyzed by flow cytometry.

The percentage of proliferating cells was then used to calculate the percent suppression of proliferation. Percent suppression of proliferation was calculated using the following formula: (1 - (% proliferation with MDSC /% proliferation without MDSC))* 100.

Lectin immunostaining

Tumors were frozen in OCT compound, then prepared in 10 µm sections on a cryostat microtome. Lectin staining was done with Griffonia Simplicifolia Lectin I (GSL I) isolectin B4 Fluorescein (Vector Laboratories) according to manufactor's protocol. Quantification was done with Image J.

Doppler imaging and quantification

Mice were shaved, anesthetized with isoflurane and kept under monitored temperature during the time of imaging. Vessel density was evaluated by laser-Doppler perfusion imaging to assess in vivo tissue perfusion in the tumor (Moor Instrument). Quantification of the vessel density was performed with MoorLDIReview V6.1 software.

2'-deoxy-2'-[18F]fluoro-D-glucose (FDG) positron emission tomography–computed tomography (PET-CT) imaging

Prior to each imaging session, mice were fasted overnight with water ad libitum. Mice were anesthetized with isoflurane (IsoVet 100%; Centravet, France) in 100% oxygen (4% isoflurane for induction; 1–2% for maintenance). Mice were weighted, and placed on a heated plate (Minerve, France). Glycemia was measured in blood drawn from the caudal ventral artery using an Accu-Chek® Aviva Nano A (Accu-Chek, France). A customized catheter with a 29 G needle (Fischer Scientific, France) connected to a 5-cm polyethylene tubing (Tygon Microbore Tubing, Cole-Parmer0.020" × 0.060"OD; Fisher Scientific, France) was installed in the lateral tail vein of the mice. 10 MBq of FDG ([Gluscan, Advanced Applied Applications, France) in 200 µl of saline solution were injected in the mice. The mice were then put back in their cages and left awake for 30 min. Mice were anesthetized again and installed in prone position in the imaging bed of the camera (NanoScan PET-CT, Mediso Medical Imaging Systems, Hungary). Respiration and body temperature were registered. Body temperature was maintained at 37°C and anesthesia was controlled on the breathing rate throughout the entire examination. CT scans were performed first using the following parameters: mode semi-circular, tension of 50 kV, 720 projections full scan, 300 ms per projection, binning 1:4. CT data were reconstructed using filtered back projection (filter : Cosine ; Cutoff : 100%). List-mode PET data were collected between 45 and 60 min post injection of FDG, binned using a 5-ns time window, a 400- to 600-keV energy window, and a 1:5 coincidence mode. In vivo PET acquisitions were reconstructed using the Tera-Tomo reconstruction engine (3D-OSEM based manufactured customized algorithm, Mediso Medical Imaging Systems, Hungary) with expectation maximization iterations, scatter and attenuation corrections. Images were analyzed using the software PMOD (PMOD Technologies LLC, Switzerland). Standardized Volume of Interest (VOI) was drawn in each organ of interest and Standardized Uptake Values (SUV) were calculated by dividing the mean tissue radioactivity concentration by the whole body concentration of the injected radioactivity. The Peak value was calculated as the maximum average SUV within a 1-cm3 spherical volume of interest and the tumor volume was automatically segmented at 33% of this value. Total FDG uptake was estimated as the product from the volume by the mean uptake of the segmented region.

Statistics

Graphs were generated and statistical analysis were performed with Prism software (GraphPad software, La Jolla). Results are expressed as means ± SEM. The Mann-Whitney t- or ANOVA tests were used as specified in the legends. Comparison between tumor growth curves have been performed using a two-way ANOVA test, and multiple comparisons have been corrected with the Bonferroni coefficient. The

association between two variables was done by spearman correlation. P values less than 0.05 was considered significant

Results

Consumption of an atherogenic diet causes low-grade systemic inflammation and accelerates murine B16-F10 melanoma tumor development in C57BL/6J mice

Genetically-modified mouse models of atherosclerosis, such as *apoe*$^{-/-}$ or *ldlr*$^{-/-}$ present a strong hypercholesterolemia. The use of an atherogenic HFHCD aggravates hypercholesterolemia and hypercholesterolemia-associated monocytosis in these mice, which accelerates the evolution of atherosclerosis [23,24]. Here we found that feeding non-transgenic C57BL/6J mice with HFHCD for 2 weeks also led, though to a lesser extent, to increased plasma cholesterol levels (1.26±0.1g/l in HFHCD-fed mice (n=10) versus 0.56±0.13g/l in control chow diet (CD)-fed mice (n=13); $P \leq 0.0001$) and monocytosis (6.8±1.6% in HFHCD-fed mice (n=8) versus 4.8±1% in control CD-fed mice (n=16); $P \leq 0.01$). Ly6C^{hi} monocytes dominated HFHCD-associated monocytosis over Ly6C^{lo} monocytes, as seen by their increased percentage and number in blood (Figure 1A). Sustained elevation of circulating Ly6C^{hi} monocytes has been identified in several pathologies as a marker of chronic inflammation with a prognostic value [25]. Based on this observation, we aimed to evaluate the role of hyperlipidemia-associated systemic low-grade inflammation on solid tumor development. We subcutaneously injected B16-F10 melanoma or TC1 tumor cells to mice under either CD or 2-week-HFHCD, and followed tumor growth for up to 15 days (Figure 1B). Mouse euthanasia was performed by cervical dislocation after anesthesia with 4% isoflurane.

We found that HFHCD significantly accelerated solid melanoma growth after 9 days of tumor development (Figure 1C, supplemental fig 1A), and increased tumor weight at day 15, when tumors reached about 200 μm^2 (Figure 1D). Similar results were observed in TC1-injected mice (Supplemental fig 1B), suggesting that the protumoral effect of the HCHFD may be applicable to other types of solid tumors. We chose to focus on the melanoma model for the rest of the study. The size of tumors positively correlated with the weight of spleens, supporting the involvement of inflammatory mechanisms in tumor growth acceleration under HFHCD (Figure 1E). We performed a transcriptome analysis at day 9 to provide valuable information about changes in gene expression at the early stages of tumorigenesis in response

to HFHCD. The most significant genes were sorted by log fold change (logFC), clustered in a hierarchical manner using the rlog differences and shown in a heatmap (Figure 2A). Notable modifications in the expression of genes involved in complement pathway, myeloid and T cell migration and genes regulating inflammation in tumors from the HFHCD group, in comparison to the CD group were observed. Clusters of expression are detailed in supplementary tables 1 and 2. VEGF-A expression was significantly increased in tumors from the HFHCD group in comparison to the CD group (figure 2B, supplemental table 2). Consistently, VEGF-A protein level was also increased in tumors from the HFHCD group (Figure 2C). VEGF-A is a key player in tumorigenesis [26] and its expression level is associated with the progression of malignant melanoma and other types of cancers [27,28]. In line with the increase of VEGF-A, microvessel density was higher in tumors of the HFHCD group (Supplemental fig 1C), suggesting an amplification of the angiogenic processes in response to HFHCD. The production of VEGF-A by tumor cells is generally stimulated by hypoxia and is associated with increased glucose metabolism [29]. We then tested whether the HFHCD directly amplified tumor cell activity *in vivo*. To this end, we measured [^{18}F] fluorodeoxyglucose (FDG) uptake by the tumor at day 9 of tumor development, using positron emission tomography–computed tomography (PET-CT). Total, but not mean intensity, FDG uptake was higher in tumors of HFHCD-fed mice compared to tumors of CD-fed mice, which was mostly attributable to the increase in tumor size rather than to a change in metabolic reprogramming of tumor cells (Supplemental Figure 1D). This suggests that the pro-atherogenic HFHCD did not directly impact the metabolic activity of tumor cells *in vivo*, and rather points to the implication of other components of the tumor microenvironment in tumor aggravation under HFHCD.

HFHCD-associated myelopoiesis accelerates the recruitment of pro-tumoral myeloid cells into the tumor microenvironment

We studied the early chronology of leukocyte accumulation in the growing melanoma of mice on CD or HFHCD. Using flow cytometry, we found a progressive accumulation of CD45$^+$ leukocytes within the growing tumors over time, showing that inflammatory cells continuously infiltrate the tumor (Figure 3A). Nevertheless, leukocytes accumulated more extensively after 7 days in tumors of mice fed a HFHCD diet, suggesting a temporal link between immune cell infiltration and tumor expansion (Figure 3A). We next characterized the accumulation of leukocyte subtypes at day 15. We found that CD11b$^+$ myeloid cells dominated the CD45$^+$ infiltrate in both groups when compared to T, B lymphocytes and NK cells (Figure 3B). Among CD11b$^+$ cells, we observed that CD11b$^+$ Ly6C$^+$ cells, which included a heterogeneous mix of CD11b$^+$ Ly6C^{hi} Ly6G$^-$ and CD11b$^+$ Ly6C^{int} Ly6G$^+$ cells significantly increased under HFHCD (Figure 3B,C). A substantial increase in CD11b$^+$ Ly6G$^-$ F4/80$^+$ macrophages was also observed in the HFHCD group in

comparison to the CD group (Figure 3B,C). Those results are recapitulated in a T-distributed stochastic neighbor embedding (t-SNE) representation (Figure 3D).

As we showed that pro-atherogenic HFHCD significantly increased Ly6C^{hi} monocyte numbers in blood (Figure 1A), we tested the hypothesis that enrichment of CD11b^{+} Ly6C^{+} cells and macrophages in the tumor of mice under HFHCD was directly linked to the circulating monocytosis. We first validated in our model that myeloid cells in the tumor derived, at least in part, from circulating blood cells. *In vivo* labeling of circulating monocytes and neutrophils was performed with intravenous injection of a combination of anti-CD115 plus anti-Ly6G in mice. After 6 hours, we found labeled monocytes in the CD11b^{+}Ly6C^{hi} population, and labeled neutrophils in the CD11b^{+}Ly6C^{int} population (Supplemental figure 2A). We next quantified monocyte infiltration in the tumor with fluorescent latex microbeads as previously shown [24,30]. Beads were injected intravenously in mice under CD and HFHCD at day 8, and tumors were harvested 24 hours later. Labeled-monocytes were found in the tumors of both groups and tended to accumulate more in tumors under HFHCD (supplemental figure 2B). Taken together, these results, which agree with the previous literature [31,32], show that circulating monocytes and neutrophils supply a substantial part of the CD11b^{+} Ly6C^{+} pool in the forming tumor, and this process is increased in condition of HFHCD.

We next sought to investigate whether myeloid cell depletion would dampen tumor growth under HFHCD. Repeated injections of clodronate liposomes were used to deplete phagocytes (Figure 4A). Ly6C^{lo} monocytes have been shown to exert higher phagocytosis capacity Clodronate liposomes depleted Ly6C^{lo} monocytes in CD and HFHCD conditions as expected. Clodronate liposomes specifically reduced the level of circulating Ly6C^{lo} in mice under CD as expected (Figure 4B), and this did not affect tumor size (Figure 4C, white bars). In contrast, the use of clodronate in HFHCD-fed mice deeply reduced the level of circulating Ly6C^{hi} monocytes in comparison with control PBS-liposome treated HFHCD-fed mice (Figure 4B) and substantially prevented tumor growth (Figure 4C, grey bars). The increased sensitivity of Ly6C^{hi} monocytes to multiple injections of clodronate liposomes in condition of HFHCD has not been reported before to our knowledge. The use of clodronate accordingly decreased the proportions of leukocytes and myeloid cells in the tumors of mice fed a HCHFD (Figure 4D). Circulating neutrophils were not efficiently depleted with clodronate and repeated injection of clodronate increased their blood levels (Supplemental figure 3). These results show that under conditions of systemic low-grade inflammation, the expansion of Ly6C^{hi} monocytes directly contributes to the early accumulation of pro-tumoral myeloid cells in the forming tumor and to tumor growth.

The loss of IL-1β or myeloid cell-derived VEGF-A recapitulates the beneficial effect of myeloid cell depletion on tumor development in mice fed a high fat/high cholesterol diet

In addition to modulating immune cell production and infiltration, pro-atherogenic HFHCD has been shown to reprogram innate immune cell phenotype, both processes being thought to contribute to inflammatory disease progression [33]. As expected, we observed that LPS±IFNγ stimulated splenocytes from HFHCD treated-mice presented a robust pro-inflammatory response as compared to mice fed a normal CD (Figure 5A). Then, we used a luminex assay to analyze the immune profile of leukocytes in the tumor microenvironment of mice under CD or HFHCD. We found that $CD45^+$ leukocytes isolated from the tumors of HFHCD-treated mice produced higher amounts of chemokines CCL5, CCL2, and CCL4 (Figure 5B), which supported our findings of increased myeloid cell recruitment in the tumor (see above). In addition, we found a significant increase of pro-inflammatory and pro-angiogenic markers TNF-α, IL-1β and VEGFR2 in conditioning media of leukocytes from the tumor of mice under HFHCD (figure 5C). These data show the emergence of a systemic pro-inflammatory immune profile in mice fed a HFHCD, which may trigger both systemic myelopoiesis and recruitment of pro-tumoral myeloid cells to the site of tumor development. We evaluated the direct role of tumor-associated immune cells on tumor cell proliferation using a co-culture assay. We isolated total $CD45^+$ cells from tumors of mice on CD or HFHCD for 9 days and co-cultured them with fresh B16-F10 melanoma cells *ex vivo*. After 24 hours of co-culture, tritiated thymidine was added to the medium in order to quantify B16-F10 proliferation capacity. Co-culture with leukocytes isolated from tumors of mice under CD significantly altered the proliferation capacity of B16-F10 cells (Figure 5D), showing that CD45+ cells can either limit tumor cell proliferation or kill tumor cells. In contrast, when co-cultured with leukocytes isolated from tumors of mice under HFHCD, B16-F10 melanoma cells kept their high proliferation capacity (Figure 5D), showing that CD45+ cells from a dyslipidemic environment favor tumor cell expansion.

We hypothesized that IL-1β might be an important actor of tumor growth acceleration in the context of a proatherogenic diet. We focused on IL-1β because we found it increased in tumor-associated leukocytes from HFHCD-fed mice (figure 5C) and because it has long been established as a central regulator of inflammation, myelopoiesis [34], vascular permeability and VEGF-mediated angiogenesis [35], all processes being most likely solicited during tumorigenesis under HFHCD. The protective role of IL-1β deficiency in the development of experimental melanoma was previously shown [36]. IL-1 β-deficient mice and control mice were subjected to the HFHCD or CD as shown in figure 6A. Interestingly, we found that IL-1β deficiency completely protected mice from tumor growth acceleration under HFHCD (Figure 6B). Because IL-1β has been shown to activate the generation and function of MDSCs, we first tested the immunosuppressive capacity of IL-1β-deficient $CD11b^+$ $Ly6C^+$ cells isolated from tumors of mice under CD or HFHCD on sensitized OT-1 CD^+8 T cells, *in vitro*. We found that HFHCD increased the immunosuppressive capacities of $CD11b^+$ $Ly6C^+$ cells independently of IL-1β (Figure 6C). This shows that $CD11b^+$ $Ly6C^+$ cells are analogous to myeloid-derived suppressor cells (MDSCs) and that their immunosuppressive functions are exacerbated under HFHCD. Because IL-1β appeared to be dispensable

for the MDSC activity in our context, we tested whether it could control the generation and accumulation of MDSC in the tumors. Therefore, we monitored immune cell ratios in the blood and tumors of IL-1β-deficient mice. We observed a strong decrease of Ly6C^{hi} and Ly6C^{lo} monocytes and neutrophils in the blood of IL-1β$^{-/-}$ mice in comparison to IL-1β$^{+/+}$ mice under HFHCD (Figure 6D), suggesting that IL-1β is necessary for monocyte production and/or mobilization in this context. IL-1β deficiency also impaired MDSC infiltration into the tumors of mice under HFHCD (Figure 6E). These results suggest that IL-1β production by immune cells controls HFHCD-associated monocytosis and subsequent accumulation of MDSCs in the tumor microenvironment, with no evidence for a direct effect on MSDC immunosuppressive activity against T cells.

Besides its direct function on myeloid cell maintenance, IL-1β has also been shown to control angiogenesis, in part by interacting with the VEGF/VEGFR pathway [37]. IL-1R signaling has been shown to induce VEGF expression and secretion in a number of cell types [38], among which classical Ly6C^{hi} monocytes [39]. Accordingly, we found a positive correlation between IL-1β release and VEGFR2 expression by tumor-isolated CD45^{+} cells (Figure 7A). We therefore hypothesized that myeloid-derived VEGF-A may directly contribute to tumor growth expansion under HFHCD through direct effect on monocyte recruitment to the tumor and regulation of angiogenesis. As mentioned above, increased VEGF-A was found in tumors of mice under HFHCD. Besides tumor cells, stromal cells and particularly myeloid cells are thought to contribute to increased gradients of VEGF-A during tumorigenesis [40,41]. We used LysMCre$^{+/-}$/VEGF$^{f/f}$ (VEGF-A$^{\Delta LysM}$) mutant mice with a specific deletion of VEGF-A in the myeloid cell compartment, and LysMCre$^{-/-}$/VEGF$^{f/f}$ (WT) as control littermate mice. Mouse weight and cholesterol levels were unaffected by VEGF-A deletion in myeloid cells (Supl Fig 4 A, B). We quantified the contribution of myeloid cells to the production of VEGF-A in the tumors. VEGF-A production was increased in tumors of WT mice fed a HFHCD, as expected (Figure 7B). Interestingly, specific deletion of VEGF-A in myeloid cells was sufficient to prevent the increase of VEGF-A in tumors under HFHCD (Figure 7B). This suggests that the increase in VEGF-A in tumors in response to HFHCD is mainly of myeloid cell origin. On the other hand, myeloid cells modestly contributed to the pool of VEGF-A in tumors of mice fed a normal CD (Figure 7B). In line with this result, we found that the absence of myeloid-derived VEGF-A inhibited tumor growth amplification in response to HFHCD and recapitulated the effect of myeloid cell depletion, suggesting that the pro-tumoral activity of myeloid cells in the context of HFHCD is VEGF-A-dependent (Figure 7C). Under CD conditions, VEGF-A deficiency in myeloid cells tended to aggravate tumor progression in mice, in line with previous studies [20], although it did not reach significance in our experimental setting. Importantly, we found a positive correlation between the levels of VEGF-A protein in the tumor and the weight of the tumor, confirming the importance of VEGF-A in tumor growth and emphasizing the crucial contribution of myeloid cells in this process (Figure 7D). Mechanistically, we found that the absence of VEGF-A in myeloid cells had no impact on myeloid cell numbers in blood and in the tumor (Supl Fig 4C), which showed that the pro-tumoral effect of myeloid VEGF-A under HFHCD did not act directly on myeloid cell supply to the tumor. We found that VEGF-A deficient myeloid cells had an exacerbated inflammatory phenotype. Stimulated VEGF-A$^{\Delta LysM}$ macrophages synthetized higher levels of

IL-1β and lower levels of IL-10, in comparison to WT mice (Supl fig 4D). This is in line with previous reports [42] and may explain the lack of protection against tumor development in CD conditions. The absence of VEGF-A in inflamed macrophages did not influence their inhibitory effect on B16-F10 proliferation, suggesting no direct effect of myeloid cells on tumor cell proliferation (Supl fig 4E). However, *in vivo* VEGF-A disruption in myeloid cells stabilized tumor vessel perfusion, as assessed by echo Doppler imaging (Figure 7E) and increased ICAM-1 total expression in the tumor in response to HFHCD (Figure 7F). Taken together, these results show that in a dyslipidemic context, IL-1β increases the pool of myeloid cells with higher immunosuppressive and pro-angiogenic functions in tumors.

Discussion

Inflammation is known to be increased in individuals with dyslipidemia and has become an interesting therapeutic target in oncology. The purpose of this work was to address the role of low-grade inflammation, as a result of dyslipidemia, on solid tumor growth. Here, we report that low-grade inflammation, caused by an atherogenic high fat/high cholesterol diet (HFHCD) and evidenced by increased monocyte level, accelerated the growth of solid melanoma in mice. Detailed phenotyping revealed that HFHCD-associated Ly6C^{hi} monocytosis directly supplied myeloid-derived cell accumulation to the growing tumor, a process controlled by IL-1β. We found that in the HFHCD context, myeloid-derived suppressor cells favored tumor growth by sustaining the infiltration of myeloid cells with higher immunosuppressive capacities and increased VEGF-A production. In support of this interpretation, we found that myeloid cells rapidly dominated the tumor's infiltrate, and to a higher extent in the HFHCD-fed group compared to the CD-fed group. We demonstrated, with tracking techniques, that neutrophils and monocytes with MDSC characteristics were both recruited into the tumor. This is in line with studies showing that MDSCs arise from circulating monocytes and neutrophils, and does not rule out the possible accumulation of resident myeloid cells or circulating precursors [43,44], which was not addressed in this study. We then used clodronate-liposomes depletion strategy to directly address the role of myeloid cells in tumor development in response to HFHCD. Repeated injection of clodronate liposomes did not deplete neutrophils but instead induced a neutrophilia both in mice fed with CD and HFHCD. This observation is in line with a recent publication [45], and emphasizes the limitation of using clodronate-liposomes treatment as experimental model for neutrophil depletion. Clodronate-induced neutrophilia did not increase tumor size, suggesting a minor role of neutrophils in melanoma growth in our model, at least upon monocyte depletion. Interestingly, under CD, clodronate liposomes decreased only circulating Ly6C^{lo}

monocytes, which were not associated with a reduction in tumor growth, showing that Ly6C^{lo} monocytes did not contribute to tumor expansion. In contrast, under HFHCD conditions, clodronate liposomes additionally decreased Ly6C^{hi} monocyte levels, which inhibited the growth of tumors. This demonstrates that Ly6C^{hi} monocytes were direct actors of tumor development. Intriguingly, chronic depletion of Ly6C^{hi} monocytes was more efficient under HFHCD than under CD conditions. This suggests an increased sensitivity of Ly6C^{hi} monocytes to clodronate under HFHCD and an exhaustion of Ly6C^{hi} monocyte precursors. Apart from a role of HFHCD on monocytosis, we found that HFHCD also increased the inflammatory profile of leukocytes and the immunosuppressive capacities of MDSCs from the tumor microenvironment. Indeed, CD45^{+} cells isolated from the tumor of HFHCD-fed mice secreted higher levels of inflammatory cytokines, chemokines and growth factors, compared to cells from CD-fed mice. This suggests the development of a more inflammatory profile of leukocytes educated in HFHCD conditions. This corroborates observations in obese patients suggesting that monocyte subsets increase their inflammatory phenotype and migration capacity [46].

Beside its undisputed effect on myeloid cells, HFHCD could also affect tumor cells. We addressed the possibility of a direct effect of HFHCD on tumor cell metabolism by using FDG-PET-CT. We did not observe any increase in mean intensity of FDG consumption in the tumor, suggesting the absence of a direct effect of HFHCD on tumor cell glucose metabolism. However, it cannot be ruled out that HFHCD could have favored tumor cell proliferation through increased consumption of cholesterol and free fatty acids, or by epigenetic modifications of oncogenes, as recently shown [47].

The model of deleterious enrichment of pathogenic myeloid cells in inflammatory tissues through a surplus and increased supply of blood monocytes has been well documented in cardiovascular pathologies such as myocardial infarction, atherosclerosis and abdominal aortic aneurysm, where resolution of inflammation is altered [48–50]. Monocyte subsets are sequentially recruited to the inflamed site, proportionally to their number in the circulation [51]. In tumorigenesis, even though the absolute count of monocytes in blood and the lymphocyte to monocyte ratio have strong prognostic value in various forms of cancer [52], the contribution of excessive monocyte production to tumor growth during dyslipidemia is unknown. Nevertheless, a very recent publication demonstrated that myocardial infarction, a clinical manifestation of dyslipidemia, accelerates breast cancer in mice through increased circulating Ly6C^{hi} monocyte levels and recruitment to tumors and through reprogramming of these monocytes to an immunosuppressive phenotype [53]. Our study corroborates these findings and reinforces the inflammatory link between cardiovascular pathologies and tumorigenesis. A few studies previously pointed out the effect of Western diet on tumorigenesis in C57BL/6J mice, but they focused on tumor cells, not on host immune cells [54,55]. In one study, the use of a diet similar to that used in our study accelerated experimental prostate tumor growth, which was attributed to increased cholesterol uptake by the proliferative tumor [54]. That study emphasized the potential benefit of managing cholesterol metabolism as an anti-tumoral approach. Several studies have been conducted, since then, to further assess the association between statin use and mortality in different types of cancer, but there is no

consensus regarding the molecular targets of the potential anti-cancer effects of statins [56]. On the other hand, the recent emergence and efficacy of immunotherapy, in particular in melanoma, as an artificial stimulation of the immune system to fight cancer cells, has led to the need of understanding how immune cells are educated in the systemic and local pro-tumoral environments. Even more recently, a growing appreciation of the potential contributions of innate immune effectors to anti-tumor immunity, especially in the context of combination immunotherapy, is leading to novel strategies to elicit a more integrated immune response against cancer. Since innate cells are central actors of the inflammatory response, it is most likely that the contribution of innate cells on tumorigenesis will be further emphasized during chronic inflammatory conditions.

In our present work, we propose for the first time the concept that silent mild-dyslipidemia without obesity creates an environment that is conducive for the accumulation of pro-tumoral myeloid cells, which facilitates tumor growth. This study paves the way to new opportunities in the field of immunotherapy, targeting Ly6C^{hi} monocytes in individuals with known low-grade inflammation, in particular in the context of mild-dyslipidemia. The importance of monocyte subsets was recently pointed out in several publications, demonstrating their importance in cancer therapy. For instance, classical Ly6C^{hi} monocytes were proposed to predict response to anti-PD-1 immunotherapy [57], and non-classical Ly6C^{lo} monocytes were thought to contribute to resistance against anti-VEGF therapies in mouse models of colorectal cancer [58]. These discoveries might even be more relevant in the context of low-grade chronic inflammation, as we found a predominant role of monocytes on tumor growth in this particular context. Importantly, our data showed that VEGF-A expression was boosted in tumors of mice on HFHCD, and that was due to excessive myeloid accumulation in the tumor microenvironment at early time points. Our results bring new elements regarding the underexplored role of myeloid-derived VEGF-A in inflammatory diseases. Myeloid-derived VEGF-A was shown to regulate angiogenesis in mouse models of lung injury [59] and melanoma [20]. Alternatively, myeloid-derived VEGF-A was shown to control inflammation independently of vasculogenic effects in granulomatous inflammation [60] and in myocardial infarction [42]. A key question raised by our study is whether IL-1β and VEGF-A contributed to tumor progression in a sequential and stage-specific manner, or in a synergic way. In the context of low-grade inflammation, our results show that inhibition of either IL-1β or VEGF-A recapitulates the anti-tumoral effect of classical monocyte depletion. This suggests the sequential contribution of IL-1β and VEGF-A in early tumorigenesis in this context. In addition, our findings suggest a negative control of VEGF-A on IL-1β production in myeloid cells, which would indicate the absence of synergistic effects. Importantly, tumor cells themselves appear as little contributors of IL-1β and VEGF-A production in early metabolic syndrome, which shows that systemic dysfunction and plasticity of the immune environment dictate the early steps of tumorigenesis. While IL-1β would maintain the production of myeloid cells and probably stimulate their production of VEGF-A, VEGF-A would shape the tumor microenvironment. Complementary upregulated cytokines and chemokines may participate in this process. In addition to modulating blood flow, we found that VEGF-A controlled the phenotype of myeloid cells. As we found that MDSCs from HFHCD fed mice presented a higher capacity of immunosuppression, it would be interesting to evaluate the link, in conditions of chronic low-grade inflammation, between VEGF-A and the expression of

inhibitory checkpoints on immune cells, as VEGF-A produced in the tumor microenvironment was recently shown to enhance expression of PD-1 and other inhibitory checkpoints involved in $CD8^+$ T cell exhaustion [61]. In view of these results, association of anti-angiogenic molecules or statins with immunomodulators of inhibitory checkpoints may be of particular interest in solid tumors in individuals with pre-metabolic syndrome status.

Declarations

Fundings

This work was supported by grants from the ARC (“Association pour la recherche sur le cancer”) and the “Ligue contre le cancer” foundations. Tartour’s laboratory is supported by the “Ligue contre le cancer” foundation.

Acknowledgments

Tartour’s laboratory is tanksful to Labex Immuno-Oncology, SIRIC CARPEM, INCA PL Bio, Fondation ARC, Foncer. *In vivo* imaging was performed at the Life Imaging Facility of Paris Descartes University (Plateforme Imageries du Vivant- PIV), supported by France Life Imaging (grant ANR-11-INBS-0006) and Infrastructures Biologie Santé. We are thankful to Pr Bertrand Tavitian and Dr Thomas Viel for their expertise in molecular imaging. We thank Pr Christian Stockmann for providing $LysMCre^{+/-}/VEGF^{f}/^{f}$ mice. We thank Dr Jean-Sebastien Silvestre and Dr Jose Vilar for their scientific contribution and help with the doppler imaging. We thank members of the Inserm UMR 970 animal facility (ERI) for animal handling and breeding.

Author contributions

TT designed in the *in vitro* experiments and highly contributed to all experiments, collected and analyzed the data and participated in the manuscript edition. BE contributed to all *in vivo* experiments. MM contributed to *in vivo* experiments and mouse genotyping. JTR did most of the experiments related to $VEGF\text{-}A^{\Delta CD11b}$ mice. NG analyzed the transcriptome data. OL helped with mouse management. HAO contributed to scientific discussions. CS gave us the $VEGF\text{-}A^{\Delta CD11b}$ mice and provided advice. ZM and AT participated to scientific discussions, provided conceptual advice and participated in the manuscript

edition. ET provided resources, analyzed the transcriptome data, provided conceptual advice and participated in the manuscript edition. SP designed and performed the experiments, analyzed the data, and wrote the manuscript.

Conflict of interest statement: The authors have declared that no conflict of interest exists.

References

1. Micucci C, Valli D, Matacchione G, Catalano A. Current perspectives between metabolic syndrome and cancer. *Oncotarget*. 2016;7(25):38959-38972. doi:10.18632/oncotarget.8341
2. Koene RJ, Prizment AE, Blaes A, Konety SH. Shared Risk Factors in Cardiovascular Disease and Cancer. *Circulation*. 2016;133(11):1104-1114. doi:10.1161/CIRCULATIONAHA.115.020406
3. Deng T, Lyon CJ, Bergin S, Caligiuri MA, Hsueh WA. Obesity, Inflammation, and Cancer. *Annu Rev Pathol*. 2016;11:421-449. doi:10.1146/annurev-pathol-012615-044359
4. Huang J, Li L, Lian J, et al. Tumor-Induced Hyperlipidemia Contributes to Tumor Growth. *Cell Rep*. 2016;15(2):336-348. doi:10.1016/j.celrep.2016.03.020
5. Alikhani N, Ferguson RD, Novosyadlyy R, et al. Mammary tumor growth and pulmonary metastasis are enhanced in a hyperlipidemic mouse model. *Oncogene*. 2013;32(8):961-967. doi:10.1038/onc.2012.113
6. Wang B, Zhuang R, Luo X, et al. Prevalence of Metabolically Healthy Obese and Metabolically Obese but Normal Weight in Adults Worldwide: A Meta-Analysis. *Horm Metab Res*. 2015;47(11):839-845. doi:10.1055/s-0035-1559767
7. Wildman RP, Muntner P, Reynolds K, et al. The obese without cardiometabolic risk factor clustering and the normal weight with cardiometabolic risk factor clustering: prevalence and correlates of 2 phenotypes among the US population (NHANES 1999-2004). *Arch Intern Med*. 2008;168(15):1617-1624. doi:10.1001/archinte.168.15.1617
8. Badoud F, Perreault M, Zulyniak MA, Mutch DM. Molecular insights into the role of white adipose tissue in metabolically unhealthy normal weight and metabolically healthy obese individuals. *FASEB J*. 2015;29(3):748-758. doi:10.1096/fj.14-263913
9. Nelson ER, Wardell SE, Jasper JS, et al. 27-Hydroxycholesterol links hypercholesterolemia and breast cancer pathophysiology. *Science*. 2013;342(6162):1094-1098. doi:10.1126/science.1241908

10. Ding X, Zhang W, Li S, Yang H. The role of cholesterol metabolism in cancer. *Am J Cancer Res*. 2019;9(2):219-227.
11. Liu C, Han T, Stachura DL, et al. Lipoprotein lipase regulates hematopoietic stem progenitor cell maintenance through DHA supply. *Nat Commun*. 2018;9(1):1310. doi:10.1038/s41467-018-03775-y
12. Tall AR, Yvan-Charvet L. Cholesterol, inflammation and innate immunity. *Nat Rev Immunol*. 2015;15(2):104-116. doi:10.1038/nri3793
13. Argyle D, Kitamura T. Targeting Macrophage-Recruiting Chemokines as a Novel Therapeutic Strategy to Prevent the Progression of Solid Tumors. *Front Immunol*. 2018;9:2629. doi:10.3389/fimmu.2018.02629
14. Feng F, Zheng G, Wang Q, et al. Low lymphocyte count and high monocyte count predicts poor prognosis of gastric cancer. *BMC Gastroenterol*. 2018;18(1):148. doi:10.1186/s12876-018-0877-9
15. Shibutani M, Maeda K, Nagahara H, et al. The peripheral monocyte count is associated with the density of tumor-associated macrophages in the tumor microenvironment of colorectal cancer: a retrospective study. *BMC Cancer*. 2017;17(1):404. doi:10.1186/s12885-017-3395-1
16. van Tuijl J, Joosten LAB, Netea MG, Bekkering S, Riksen NP. Immunometabolism orchestrates training of innate immunity in atherosclerosis. *Cardiovasc Res*. 2019;115(9):1416-1424. doi:10.1093/cvr/cvz107
17. Fahey E, Doyle SL. IL-1 Family Cytokine Regulation of Vascular Permeability and Angiogenesis. *Front Immunol*. 2019;10:1426. doi:10.3389/fimmu.2019.01426
18. Mohr T, Haudek-Prinz V, Slany A, Grillari J, Micksche M, Gerner C. Proteome profiling in IL-1β and VEGF-activated human umbilical vein endothelial cells delineates the interlink between inflammation and angiogenesis. *PLoS ONE*. 2017;12(6):e0179065. doi:10.1371/journal.pone.0179065
19. Winkler F, Kozin SV, Tong RT, et al. Kinetics of vascular normalization by VEGFR2 blockade governs brain tumor response to radiation: role of oxygenation, angiopoietin-1, and matrix metalloproteinases. *Cancer Cell*. 2004;6(6):553-563. doi:10.1016/j.ccr.2004.10.011
20. Klose R, Krzywinska E, Castells M, et al. Targeting VEGF-A in myeloid cells enhances natural killer cell responses to chemotherapy and ameliorates cachexia. *Nat Commun*. 2016;7:12528. doi:10.1038/ncomms12528
21. Bent R, Moll L, Grabbe S, Bros M. Interleukin-1 Beta-A Friend or Foe in Malignancies? *Int J Mol Sci*. 2018;19(8). doi:10.3390/ijms19082155
22. Ridker PM, MacFadyen JG, Thuren T, et al. Effect of interleukin-1β inhibition with canakinumab on incident lung cancer in patients with atherosclerosis: exploratory results from a randomised, double-blind, placebo-controlled trial. *Lancet*. 2017;390(10105):1833-1842. doi:10.1016/S0140-6736(17)32247-X
23. Getz GS, Reardon CA. Diet and murine atherosclerosis. *Arterioscler Thromb Vasc Biol*. 2006;26(2):242-249. doi:10.1161/01.ATV.0000201071.49029.17
24. Combadière C, Potteaux S, Rodero M, et al. Combined inhibition of CCL2, CX3CR1, and CCR5 abrogates Ly6C(hi) and Ly6C(lo) monocytosis and almost abolishes atherosclerosis in

hypercholesterolemic mice. *Circulation*. 2008;117(13):1649-1657. doi:10.1161/CIRCULATIONAHA.107.745091

25. Yang J, Zhang L, Yu C, Yang X-F, Wang H. Monocyte and macrophage differentiation: circulation inflammatory monocyte as biomarker for inflammatory diseases. *Biomark Res*. 2014;2(1):1. doi:10.1186/2050-7771-2-1
26. Hanahan D, Weinberg RA. The hallmarks of cancer. *Cell*. 2000;100(1):57-70. doi:10.1016/s0092-8674(00)81683-9
27. Kut C, Mac Gabhann F, Popel AS. Where is VEGF in the body? A meta-analysis of VEGF distribution in cancer. *Br J Cancer*. 2007;97(7):978-985. doi:10.1038/sj.bjc.6603923
28. Rajabi P, Neshat A, Mokhtari M, Rajabi MA, Eftekhari M, Tavakoli P. The role of VEGF in melanoma progression. *J Res Med Sci*. 2012;17(6):534-539.
29. Niccoli Asabella A, Di Palo A, Altini C, Ferrari C, Rubini G. Multimodality Imaging in Tumor Angiogenesis: Present Status and Perspectives. *Int J Mol Sci*. 2017;18(9). doi:10.3390/ijms18091864
30. Cortez-Retamozo V, Etzrodt M, Newton A, et al. Angiotensin II drives the production of tumor-promoting macrophages. *Immunity*. 2013;38(2):296-308. doi:10.1016/j.immuni.2012.10.015
31. Gabrilovich DI. Myeloid-Derived Suppressor Cells. *Cancer Immunol Res*. 2017;5(1):3-8. doi:10.1158/2326-6066.CIR-16-0297
32. Lecot P, Sarabi M, Pereira Abrantes M, et al. Neutrophil Heterogeneity in Cancer: From Biology to Therapies. *Front Immunol*. 2019;10:2155. doi:10.3389/fimmu.2019.02155
33. Christ A, Günther P, Lauterbach MAR, et al. Western Diet Triggers NLRP3-Dependent Innate Immune Reprogramming. *Cell*. 2018;172(1-2):162-175.e14. doi:10.1016/j.cell.2017.12.013
34. Mitroulis I, Ruppova K, Wang B, et al. Modulation of Myelopoiesis Progenitors Is an Integral Component of Trained Immunity. *Cell*. 2018;172(1-2):147-161.e12. doi:10.1016/j.cell.2017.11.034
35. Torisu H, Ono M, Kiryu H, et al. Macrophage infiltration correlates with tumor stage and angiogenesis in human malignant melanoma: possible involvement of TNFalpha and IL-1alpha. *Int J Cancer*. 2000;85(2):182-188.
36. Voronov E, Shouval DS, Krelin Y, et al. IL-1 is required for tumor invasiveness and angiogenesis. *Proc Natl Acad Sci USA*. 2003;100(5):2645-2650. doi:10.1073/pnas.0437939100
37. Torisu H, Ono M, Kiryu H, et al. Macrophage infiltration correlates with tumor stage and angiogenesis in human malignant melanoma: possible involvement of TNFalpha and IL-1alpha. *Int J Cancer*. 2000;85(2):182-188.
38. Alagappan VKT, McKay S, Widyastuti A, et al. Proinflammatory cytokines upregulate mRNA expression and secretion of vascular endothelial growth factor in cultured human airway smooth muscle cells. *Cell Biochem Biophys*. 2005;43(1):119-129. doi:10.1385/CBB:43:1:119
39. Chittezhath M, Dhillon MK, Lim JY, et al. Molecular profiling reveals a tumor-promoting phenotype of monocytes and macrophages in human cancer progression. *Immunity*. 2014;41(5):815-829.

doi:10.1016/j.immuni.2014.09.014

40. Lewis JS, Landers RJ, Underwood JC, Harris AL, Lewis CE. Expression of vascular endothelial growth factor by macrophages is up-regulated in poorly vascularized areas of breast carcinomas. *J Pathol*. 2000;192(2):150-158. doi:10.1002/1096-9896(2000)9999:9999<::AID-PATH687>3.0.CO;2-G
41. Dewing D, Emmett M, Pritchard Jones R. The Roles of Angiogenesis in Malignant Melanoma: Trends in Basic Science Research over the Last 100 Years. *ISRN Oncol*. 2012;2012:546927. doi:10.5402/2012/546927
42. Howangyin K-Y, Zlatanova I, Pinto C, et al. Myeloid-Epithelial-Reproductive Receptor Tyrosine Kinase and Milk Fat Globule Epidermal Growth Factor 8 Coordinately Improve Remodeling After Myocardial Infarction via Local Delivery of Vascular Endothelial Growth Factor. *Circulation*. 2016;133(9):826-839. doi:10.1161/CIRCULATIONAHA.115.020857
43. Ostrand-Rosenberg S, Fenselau C. Myeloid-Derived Suppressor Cells: Immune-Suppressive Cells That Impair Antitumor Immunity and Are Sculpted by Their Environment. *J Immunol*. 2018;200(2):422-431. doi:10.4049/jimmunol.1701019
44. Kumar V, Patel S, Tcyganov E, Gabrilovich DI. The Nature of Myeloid-Derived Suppressor Cells in the Tumor Microenvironment. *Trends Immunol*. 2016;37(3):208-220. doi:10.1016/j.it.2016.01.004
45. Bader JE, Enos RT, Velázquez KT, et al. Repeated clodronate-liposome treatment results in neutrophilia and is not effective in limiting obesity-linked metabolic impairments. *Am J Physiol Endocrinol Metab*. 2019;316(3):E358-E372. doi:10.1152/ajpendo.00438.2018
46. Devêvre EF, Renovato-Martins M, Clément K, Sautès-Fridman C, Cremer I, Poitou C. Profiling of the three circulating monocyte subpopulations in human obesity. *J Immunol*. 2015;194(8):3917-3923. doi:10.4049/jimmunol.1402655
47. Atala A. Re: High-Fat Diet Fuels Prostate Cancer Progression by Rewiring the Metabolome and Amplifying the MYC Program. *J Urol*. 2020;203(5):886. doi:10.1097/JU.0000000000000781.02
48. Mellak S, Ait-Oufella H, Esposito B, et al. Angiotensin II mobilizes spleen monocytes to promote the development of abdominal aortic aneurysm in Apoe-/- mice. *Arterioscler Thromb Vasc Biol*. 2015;35(2):378-388. doi:10.1161/ATVBAHA.114.304389
49. Dutta P, Courties G, Wei Y, et al. Myocardial infarction accelerates atherosclerosis. *Nature*. 2012;487(7407):325-329. doi:10.1038/nature11260
50. Swirski FK, Libby P, Aikawa E, et al. Ly-6Chi monocytes dominate hypercholesterolemia-associated monocytosis and give rise to macrophages in atheromata. *J Clin Invest*. 2007;117(1):195-205. doi:10.1172/JCI29950
51. Nahrendorf M, Swirski FK, Aikawa E, et al. The healing myocardium sequentially mobilizes two monocyte subsets with divergent and complementary functions. *J Exp Med*. 2007;204(12):3037-3047. doi:10.1084/jem.20070885
52. Schmidt H, Bastholt L, Geertsen P, et al. Elevated neutrophil and monocyte counts in peripheral blood are associated with poor survival in patients with metastatic melanoma: a prognostic model. *Br J Cancer*. 2005;93(3):273-278. doi:10.1038/sj.bjc.6602702

53. Koelwyn GJ, Newman AAC, Afonso MS, et al. Myocardial infarction accelerates breast cancer via innate immune reprogramming. *Nat Med*. Published online July 13, 2020. doi:10.1038/s41591-020-0964-7
54. Llaverias G, Danilo C, Wang Y, et al. A Western-type diet accelerates tumor progression in an autochthonous mouse model of prostate cancer. *Am J Pathol*. 2010;177(6):3180-3191. doi:10.2353/ajpath.2010.100568
55. Kimura Y, Sumiyoshi M. High-fat, high-sucrose, and high-cholesterol diets accelerate tumor growth and metastasis in tumor-bearing mice. *Nutr Cancer*. 2007;59(2):207-216. doi:10.1080/01635580701499537
56. Fatehi Hassanabad A. Current perspectives on statins as potential anti-cancer therapeutics: clinical outcomes and underlying molecular mechanisms. *Transl Lung Cancer Res*. 2019;8(5):692-699. doi:10.21037/tlcr.2019.09.08
57. Krieg C, Nowicka M, Guglietta S, et al. High-dimensional single-cell analysis predicts response to anti-PD-1 immunotherapy. *Nat Med*. 2018;24(2):144-153. doi:10.1038/nm.4466
58. Jung K, Heishi T, Khan OF, et al. Ly6Clo monocytes drive immunosuppression and confer resistance to anti-VEGFR2 cancer therapy. *J Clin Invest*. 2017;127(8):3039-3051. doi:10.1172/JCI93182
59. Stockmann C, Kerdiles Y, Nomaksteinsky M, et al. Loss of myeloid cell-derived vascular endothelial growth factor accelerates fibrosis. *Proc Natl Acad Sci USA*. 2010;107(9):4329-4334. doi:10.1073/pnas.0912766107
60. Harding JS, Herbath M, Chen Y, et al. VEGF-A from Granuloma Macrophages Regulates Granulomatous Inflammation by a Non-angiogenic Pathway during Mycobacterial Infection. *Cell Rep*. 2019;27(7):2119-2131.e6. doi:10.1016/j.celrep.2019.04.072
61. Voron T, Colussi O, Marcheteau E, et al. VEGF-A modulates expression of inhibitory checkpoints on CD8+ T cells in tumors. *J Exp Med*. 2015;212(2):139-148. doi:10.1084/jem.20140559

Figures

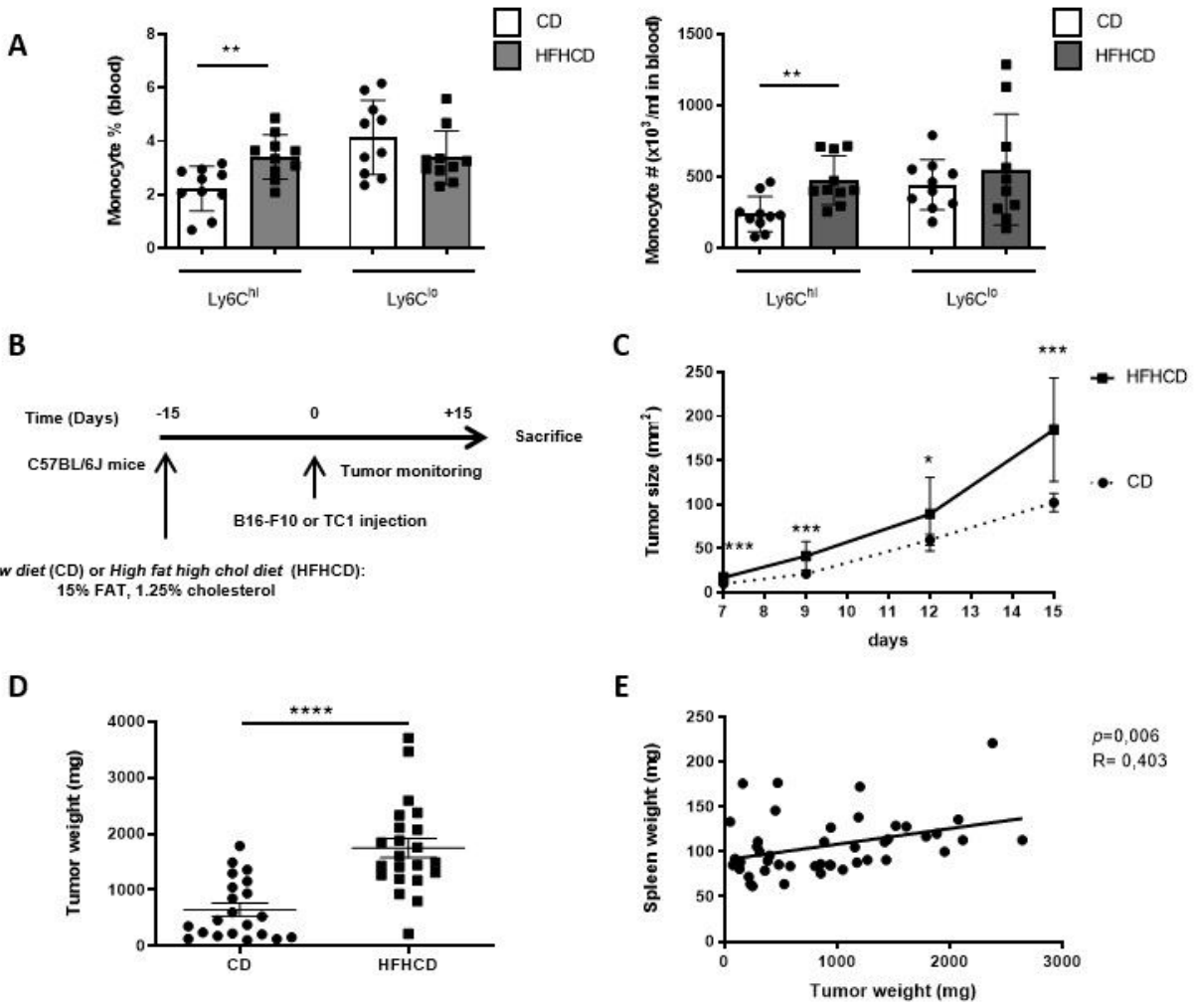

Figure 1

Pro-atherogenic high fat high cholesterol diet (HFHCD) accelerates B16-F10 melanoma growth in C57BL/6J mice A) Monocyte subsets in blood of mice fed a CD or a HFHCD for 15 days assessed by flow cytometry. Left: percentages, right: absolute numbers. B) Protocol design of the experiment: C57BL/6J mice were fed with regular chow diet (CD) or pro-atherogenic high fat high cholesterol diet (HFHCD) for 2 weeks and challenged with 0.25x106 B16-F10 melanoma or TC1 cells (results in Sup Fig 1B) subcutaneously injected. The diet was maintained until the end of experiment. Mice were sacrificed up to day 15. C) Tumor size monitoring over time. Unpaired t-test. *p<0.05, * * p<0.01, * * * p<0.001 D) Tumor weights at the time of sacrifice. E) Correlation between spleen and tumor weight (n=21-22 mice/group). Spearman correlation (E). Mean±sem. Mann-Whitney t-test. *p<0.05 *p<0.05,***p<0.001 (A,D).

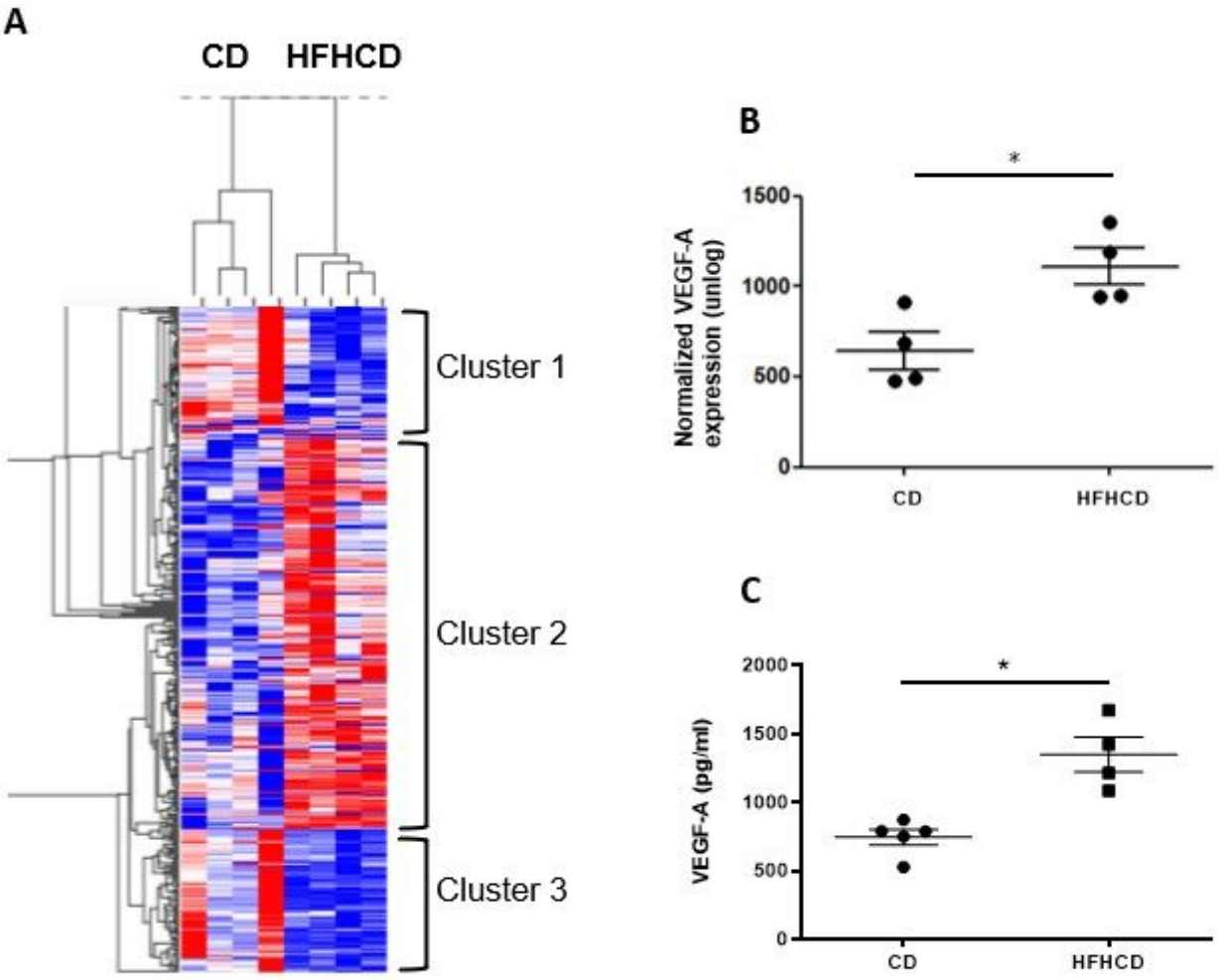

Figure 2

Transcriptomic analysis of melanoma tumors from CD versus HFHCD-treated mice. A) Heat map of gene expression analysis on RNA extract from tumor of mice under CD or HFHCD at day 9 post B16-F10 cell injection (n=4 mice/groupe). Clusters are detailled in supplemental tables. B) Differential normalises VEGF-A expression was shown in CD vs HFHCD mice (mean +/- SEM ; t-test p-value). C) VEGF-A level measured in whole tumor lysate by ELISA. Mean±sem. Mann-Whitney t-test *p<0.05

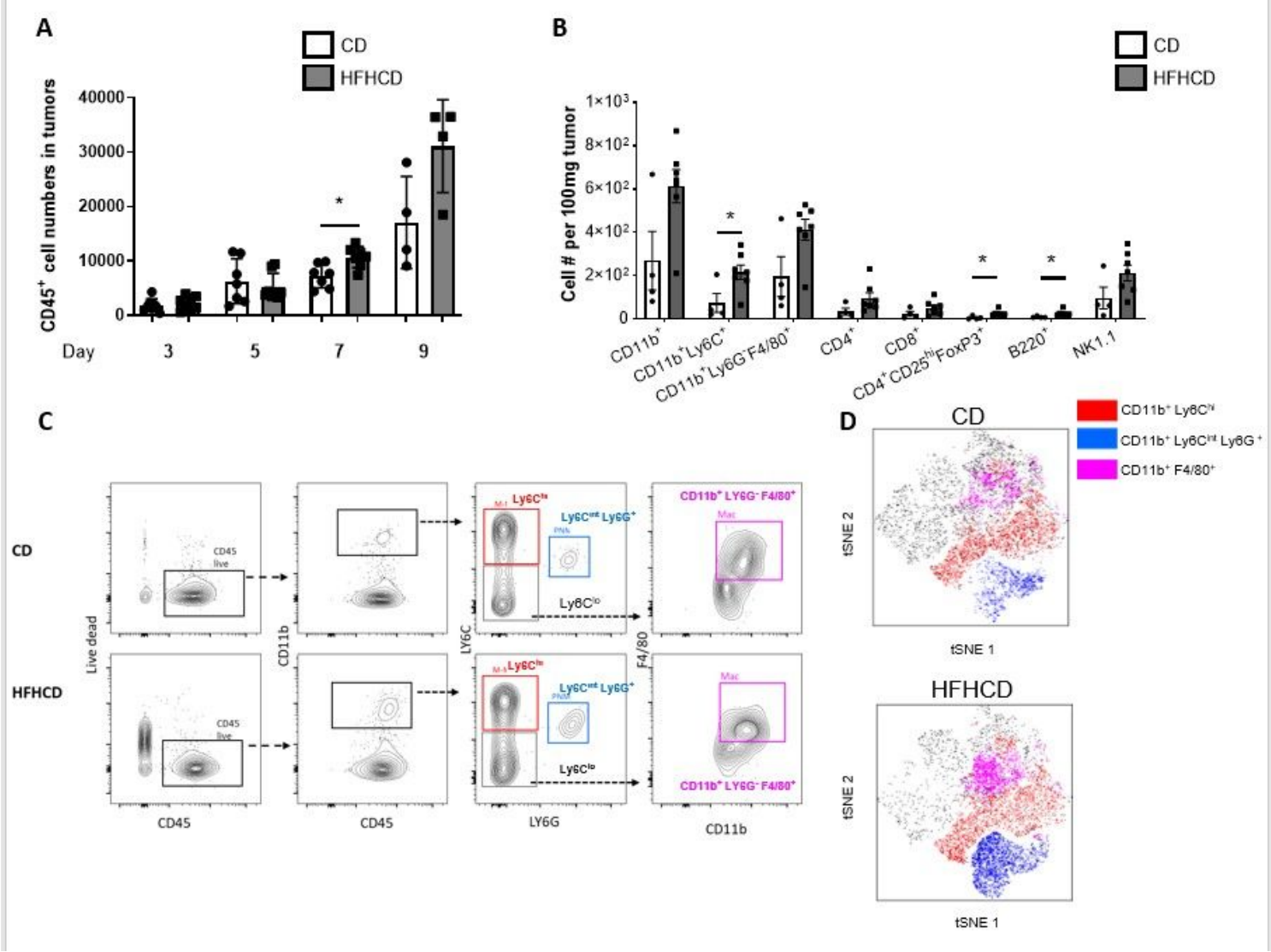

Figure 3

HFHCD accelerates the accumulation of myeloid cells in the tumor microenvironment B16-F10 cells were implanted subcutaneously into C57BL6/J mice, fed with CD or HFHCD for 2 weeks. Diet was maintained until the end of experiment. A) Kinetic of CD45+ leukocyte accumulation in the tumor microenvironment assessed by flow cytometry (n=4-8 mice/group, 2 independent experiments combined). B) On day 15, tumors were harvested, tumor-infiltrating immune cells were counted and analyzed by flow cytometry. Total numbers of immune cell infiltration were showed (n=4-7 mice/group from one representative experiment). C) Gating strategy for myeloid cells in tumors D) Single live CD45 cells from the flow cytometry data of tumors were concatenated and subjected to the t-SNE dimensional reduction. CD11b expression in CD or HFHCD tumors are colored mapped from blue (low expression) to red (high expression) into the t-SNE map. CD11b+Ly6Chi, CD11b+Ly6CintLy6G+, CD11b+F4/80+ populations were overlayed into the t-SNE map. Mean±sem. Mann-Whitney t-test. *p<0.05

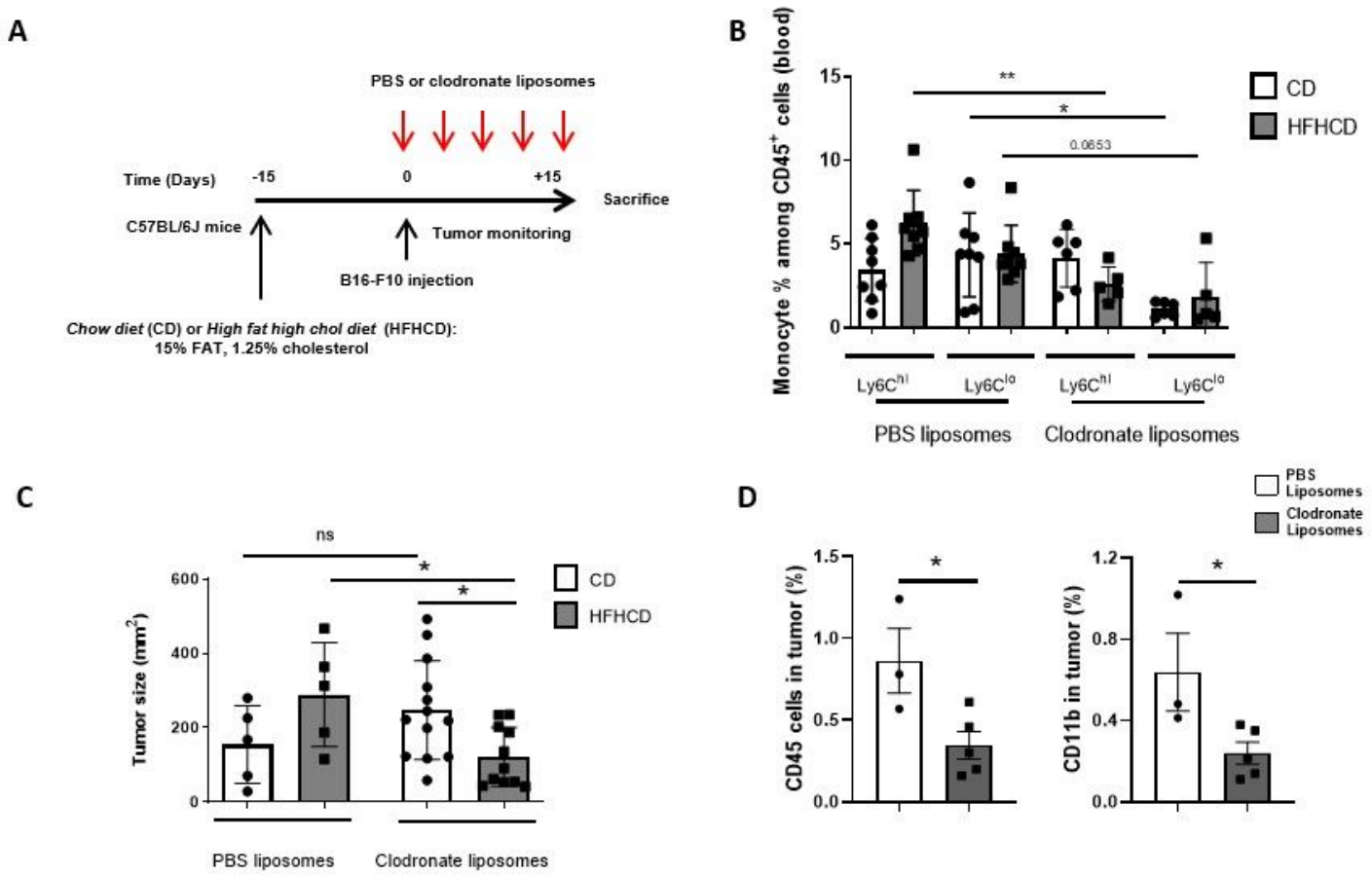

Figure 4

Depletion of myeloid cells prevents accelerated tumor growth under HFHCD diet C57BL/6J mice, fed with CD or HFHCD for 2 weeks, were transplanted subcutaneously with 0,25x106 B16-F10 cells (D0) and treated with clodronate liposomes or PBS liposomes every 3 days from D0 until end of experiment (200mg ip). Diet was maintained until the end of experiment. A) Protocol design of the experiment. B-D) Mice were sacrificed on day 15 days post B16-F10 injection, B) Monocyte subsets (CD11b+Ly6C hi/lo) were monitored in blood. Mean±sem. Mann-Whitney t-test.*p<0.05,**p<0.01 (n=5-8 mice/group from one representative experiment). C) Tumor size at day 15 (n=5-12 mice/group, 2 independent experiments pooled). Mean±sem. Mann-Whitney t-test.*p<0.05 D) Percentage of total leukocytes and subsets of myeloid cells in tumors of mice under HFHCD analyzed by flow cytometry at day 15 (n=3-5 mice/group from one representative experiment). Mean±sem. Unpaired t-test. *p<0.05

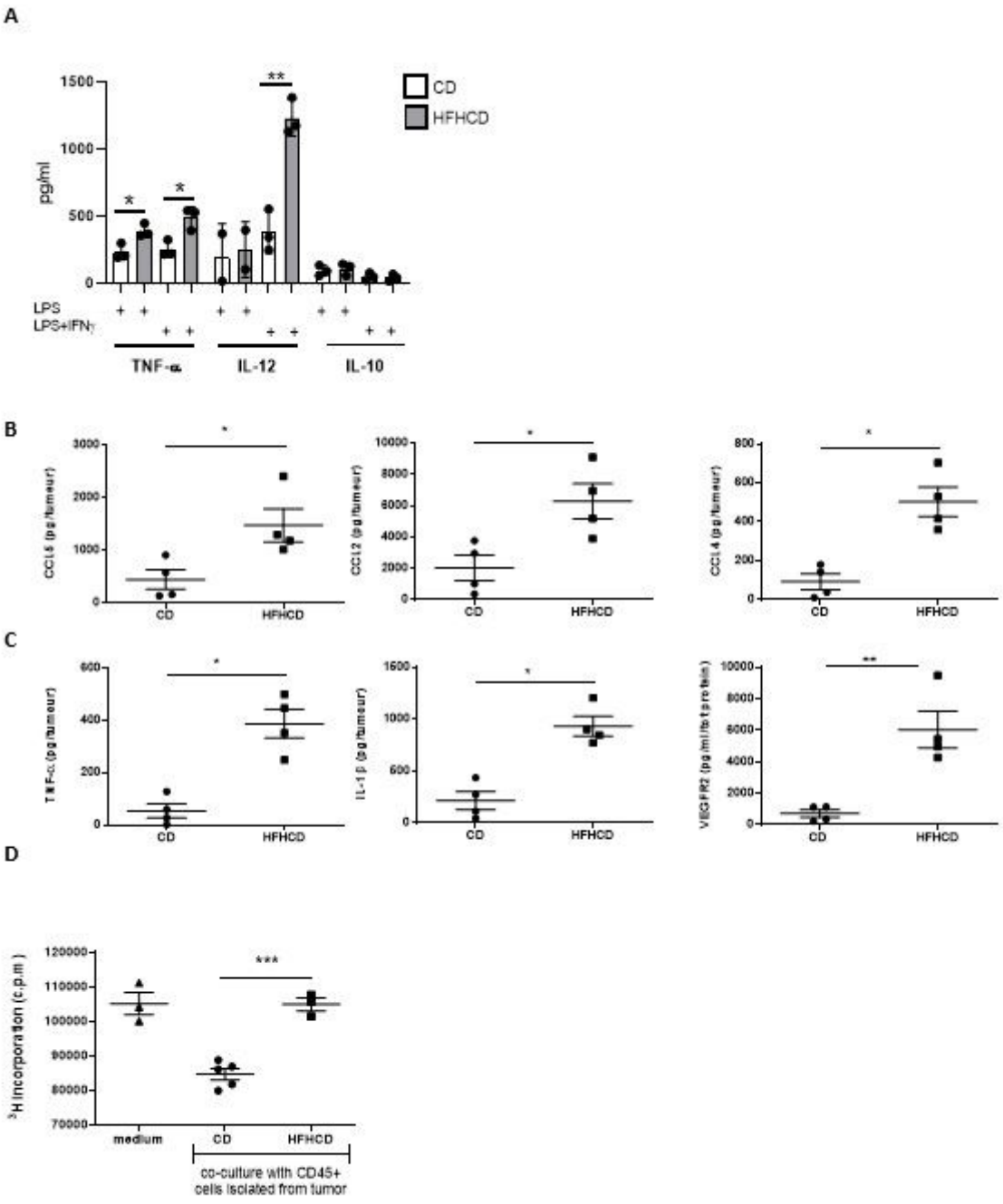

Figure 5

HFHCD educates leukocytes to become pro-inflammatory in systemic and in the tumor microenvironment 0,25x106 B16-F10 cells were implanted subcutaneously into C57BL6/J mice, fed with CD or HFHCD for 2 weeks. Diet was maintained until the end of experiment. A) Splenocytes from CD and HFHCD-fed mice were stimulated in vitro with LPS (10ug/ml) +/- IFNγ (100UI/ml) for 24 hours. Cytokine secretion was measured in the supernatant by ELISA. Unpaired t-test. *p<0.05, * * p<0.01 B-C) CD45+cells were isolated from B16-F10 tumors at day 15 post-injection. And cultured in medium for 24h. Chemokines (B),

inflammatory and angiogenic factors (C) were measured in the medium by ELISA or Luminex assay (n=4/group). D) B16-F10 cell line (10 000 cells/well) was co-cultured with CD45 cells (2 500 cells/wells) for 24h. B16-F10 proliferation was measured by 3H-Thymidine incorporation (n=3-5/group). Mean±sem. Mann-Whitney t-test.*p<0.05,**p<0.01,***p<0.001 (B-D)

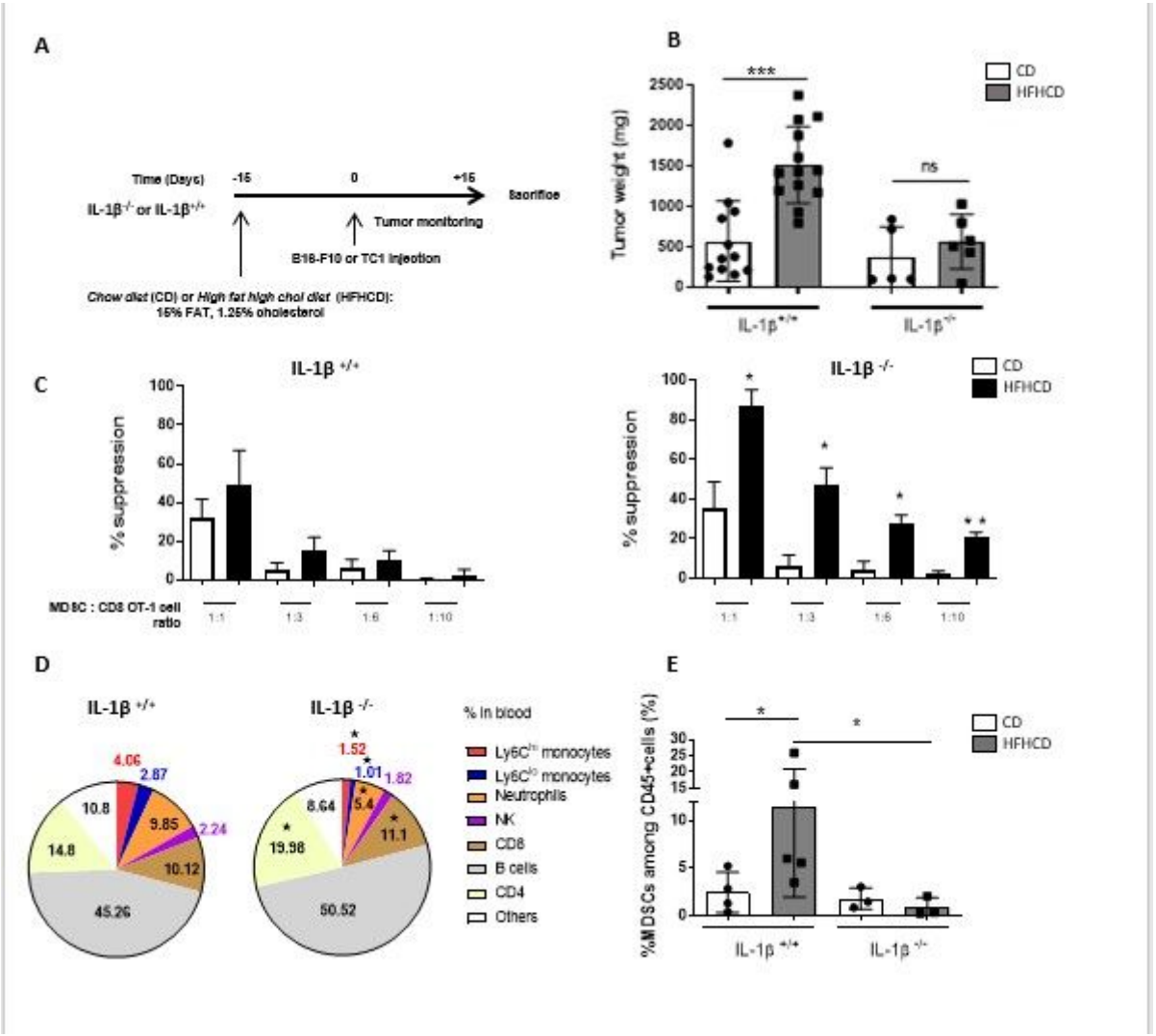

Figure 6

: IL-1β deficiency prevents tumor growth and MDSCs infiltration under HFHCD IL-1β-/- mice and their control IL-1β+/+mice were fed for 2 weeks with CD or HFHCD, and were transplanted subcutaneously with 0,25x106 B16-F10 cells. Diet was maintained until the end of experiment. Mice were sacrificed at day 15 post injection. A) Protocol design of the experiment. B)Tumor weight (n=5-13 mice/group, 2 independent experiments combined) C) Suppressive activity of myeloid-derived suppressor cells (MDSC) was evaluated by CFSE dilution in CD8+ OT-I T cells in the presence of OVA257-264 (SIINFEKL) and titrated MDSCs isolated from tumors of IL-1β+/+ or IL-1β-/- mice. Proliferation was measured after 72 hours by flow cytometry. (n=3-4/group).D) Proportion of immune cells in blood of mice under HFHCD (n=5-7/group, statistical difference between the 2 groups, for the same leukocyte subset, was mentioned on the pie chart by *). E) MDSC in tumors were analyzed by flow cytometry (n=3-5 mice/group from 1

representative experiment). Mean±sem. Mann-Whitney t-test (A, D) or Anova Test with Tukey's multiple comparison test.*p<0.05,**p<0.01,***p<0.001 (C, E)

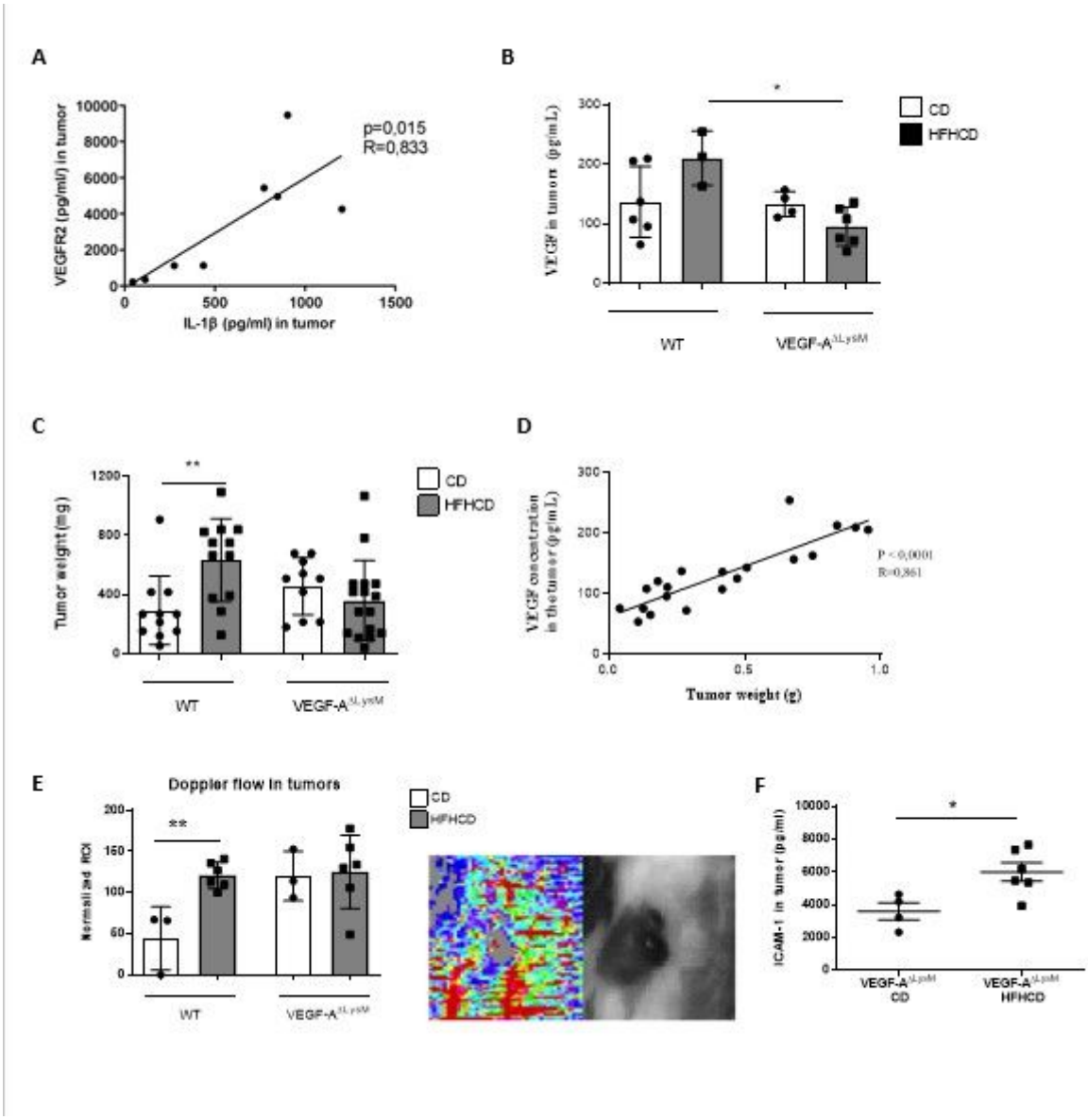

Figure 7

Inhibition of VEGF production by myeloid cells prevents tumor growth under HFHCD A) Correlation of VEGFR2 with IL-1β production in B16-F10 tumor C57BL6/J mice fed with CD or HFHCD. B-F) LysMCre+/-/VEGFf/f (VEGF-A LysM) and their control littermate LysMCre-/-/VEGFf/f (WT) mice were fed for 2 weeks with CD or HFHCD, and were transplanted subcutaneously with 0,25x106 B16-F10 cells. Diet was maintained until the end of experiment. Mice were sacrificed at day 15 post injection. B) VEGF-A production in tumors measured by ELISA (n=3-6/group). C) Tumors weight (n=11-16 mice/group, 2 independent experiments combined). D) Correlation of VEGF-A concentration in tumor with tumor weight. E) Laser Doppler perfusion imaging (PDPI) of tumors at day 9 (Right: representative picture). Mice were positioned on their back on a light-absorbing pad. LDPI image post-processing and measurement standardized protocol: the mean intensity of the Doppler signal was registered in ROI (Region of interest) encompassing the tumor and expressed as numerical value normalized for their area. (n=3-6

mice/group). F) ICAM-1 level measured in tumors by Luminex assay (n=4-6/group). Mean±sem. Mann-Whitney t-test (B,C,E,F). Spearman correlation (A,D). *p<0.05,***p<0.001

Supplementary Files

This is a list of supplementary files associated with this preprint. Click to download.

- Graphicalabstract.pdf
- supltable1.pdf
- supltable2.pdf
- s1.jpg
- s2.jpg
- s3.jpg
- s4.jpg